Operator effective medium approximation for inhomogeneous and curvilinear media

Andrey Novitsky [1,2,*] Milena Ramanovich [1,3] and Denis V. Novitsky [3]

[1] *Department of Physical Optics and Applied Informatics, Belarusian State University, Nezavisimosti Avenue 4, 220030 Minsk, Belarus*

[2] *Department of Physics and Engineering, ITMO University, Kronverksky Prospekt 49, 197101 St. Petersburg, Russia*

[3] *B. I. Stepanov Institute of Physics, National Academy of Sciences of Belarus, Nezavisimosti Avenue 68-2, 220072 Minsk, Belarus*

(Received 23 August 2023; revised 25 September 2023; accepted 19 October 2023; published 1 November 2023)

Effective medium theory is an integral part of the area of metamaterials providing insights into the physics behind their interaction with light. In this paper, we develop the operator effective medium approximation for spherical and cylindrical multilayer systems. Equating evolution operators (wave propagators) for the actual multilayer and homogenized medium, we establish the effective material parameters, which differ for planar and curvilinear cases. We supplement the criterion for applicability of the effective medium approximation with the assertion that the radii of curvilinear layers must be about or greater than the radiation wavelength. The operator effective medium approximation provides a clear way to approach nonlocal corrections, as well as characterize structures with balanced loss and gain. We envisage that the operator effective medium approximation will be useful for the characterization of metamaterials and other nanophotonic systems of complex shapes.

DOI: 10.1103/PhysRevB.108.205401

I. INTRODUCTION

Microstructure of a substance can be disregarded, if a wave cannot recognize a single atom in a material. In this case, the wavelength embraces many atoms validating the continuous medium approximation. The latter can be also applied for man-made composite materials — metamaterials [1–3] with the building blocks (meta-atoms) much bigger than the natural atoms. Therefore the spectral range of metamaterial operation shifts to longer wavelengths. Materials and shapes of meta-atoms as well as specific lattice symmetries of their arrangement specify the featuring response of metamaterials.

There are different techniques to approach effective material parameters within the continuous medium approximation, if one starts from the microstructure of a metamaterial [4,5]. Homogenization is essential, for example, to understand how artificial magnetism arises in a structure composed of nonmagnetic materials. For homogenization, one can exploit just a mixing rule, when several types of particles are available. If the amount of one sort of particles is much greater than that of the others, then the Maxwell Garnett approximation is applicable [6–9]. However, if the amounts of particles are comparable, the Bruggeman approach should be employed. Maxwell-Garnett-like approximation as a mixing rule is also used for homogenization of planar layered systems [10–15]. It is surprising that such an intuitive technique assumed to be always valid in the long wavelength regime can be misleading in specific conditions such as under the critical angle of total internal reflection resulting in the effective medium approximation (EMA) breakdown. Effective medium of a multilayer system is commonly treated as a homogeneous anisotropic one, the information on the actual distribution of materials being ignored. The latter assertion means that the system is described by local effective material tensors. If the distribution of materials is involved in the description, then it becomes more accurate at the price of nonlocal effective material tensors depending on the radiation wave vector [16]. One can expect a similar EMA for cylindrically and spherically symmetric multilayer systems, but the curvature of layers might dramatically change the conditions for EMA. Effective material parameters of a spherical nanoparticle can be also determined using the so called internal homogenization approach based on averaging polarizabilities of particle's core and shell [17].

In order to find the adequate effective material tensors of the metamaterial composed of rods or spheres, the coherent potential approximation was proposed [18–23]. This approach is based on the idea that when placing the meta-atoms to the medium with the required effective parameters, they do not scatter light. The effective parameters can be retrieved from such no-scattering conditions. This approach describes a metamaterial as a nonlocal medium as well. In general, the first-principle approaches might be used based on the multipole expansion of periodic metamaterial's response [24–26]. In the particular case of meta-atoms as electric dipolar scatterers, it was proved that the nonlocal effective material parameters are better suited for describing metamaterials with the unit cells comparable to the radiation wavelength [27]. Taking into account contributions of multipolar meta-atoms in a lattice, it is possible to get effective dielectric permittivity, magnetic permeability, magnetoelectric coefficients, as well as nonlinear susceptibilities [28–31]. Recent progress in the study of low-dimensional materials allows engineering electric and magnetic surface conductivities and metamaterials with arbitrary effective material parameters [32,33]. Effective material parameters can be also retrieved from either experimental or numerical data [34–39]. The relations of the reflection and transmission coefficients make possible to determine the effective material parameters, the adequacy of

*andreyvnovitsky@gmail.com

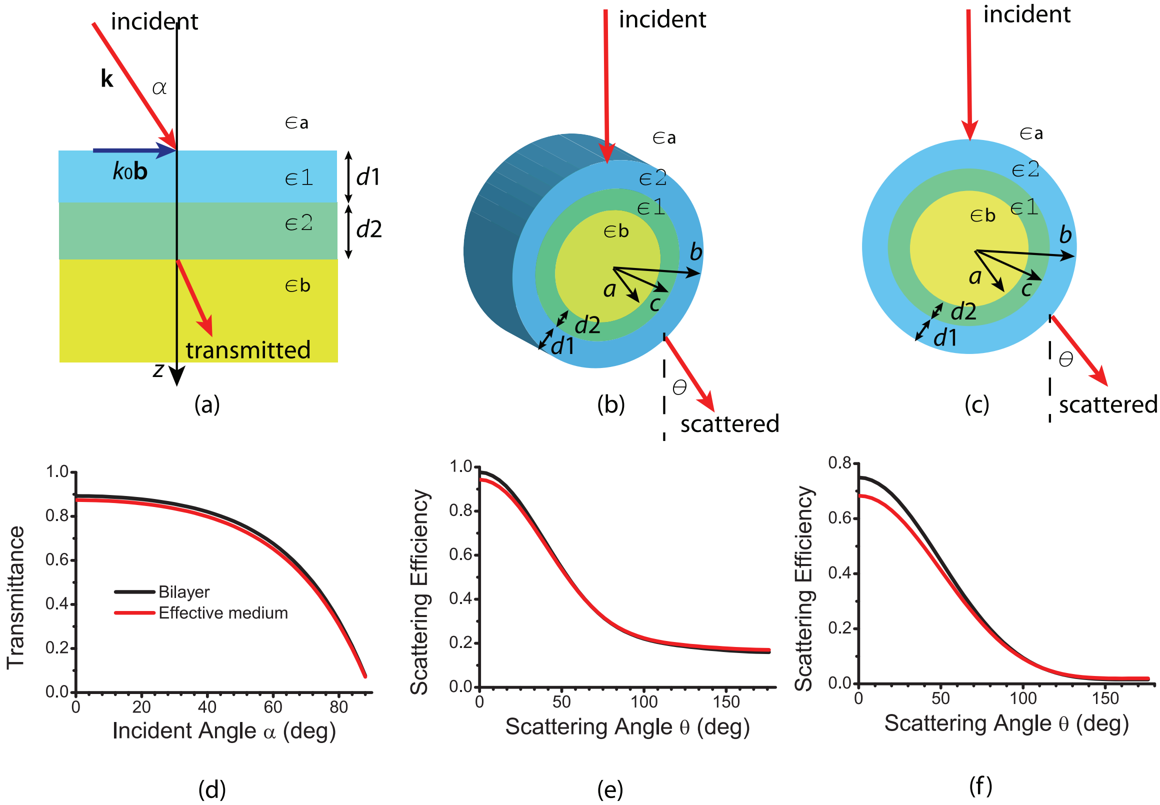

FIG. 1. [(a)–(c)] Three basic geometries in question: planar, cylindrical, and spherical, respectively. Comparison of scattered characteristics for (d) planar ($\varepsilon_1 = 5$ and $\varepsilon_2 = 1$), (e) cylindrical ($\varepsilon_1 = 1$ and $\varepsilon_2 = 5$), and (f) spherical ($\varepsilon_1 = 1$ and $\varepsilon_2 = 5$) bilayer structures versus the corresponding effective media. Parameters: $\varepsilon_a = 1$, $\varepsilon_b = 5$, thicknesses of layers $d_1 = d_2 = 10$ nm, inner radius of the cylindrical and spherical systems $a = \lambda/2\pi$, and wavelength $\lambda = 500$ nm.

which depends on the *a priori* knowledge of the supposed effective medium properties, whether it is magnetic, anisotropic, chiral, etc.

In this paper, we develop the effective medium approach beyond the ordinary planar multilayer systems sketched in Fig. 1(a). We achieve this using the general operator technique to find the scattered electromagnetic fields for cylindrical and spherical multilayered systems [see Figs. 1(b) and 1(c)]. The generic operator approach allows reducing the Maxwell equations to the set of ordinary differential equations due to symmetry of the fields. Fundamental solution of this set of equations can be represented as the spatial evolution operator. With the concept of evolution operators, it is possible to expand the operator effective medium approximation beyond homogenization of planar multilayers reported earlier [16,40]. In particular, we extend the operator effective medium theory to cylindrically and spherically symmetric multilayers. In Figs. 1(d)–1(f), one can see that the scattering efficiency for curvilinear EMA noticeably departures from that of the multilayer even for deeply subwavelength layers. This poses a problem of closer investigation of the curvilinear EMA and the limits of its applicability.

The paper is organized as follows. Section II introduces a reader to the operator EMA for systems of planar layers. The homogenization theory developed in Ref. [16] is generalized to continuously distributed inhomogeneous media. In Secs. III and IV, this idea is employed to determine the effective permittivity tensors of homogenized spherical and cylindrical multilayers. In Sec. V, we demonstrate how the corrections to the effective material parameters can be found. We extract material parameters of a bilayer with balanced loss and gain in Sec. VI. Section VII concludes the paper.

II. OPERATOR EFFECTIVE MEDIUM APPROXIMATION FOR INHOMOGENEOUS PLANAR LAYERS

First, we remind the operator EMA developed in Ref. [16] for a stack of planar layers. To this end, we consider propagation of a monochromatic plane wave in a layer, the angular frequency being equal to ω. Incident angle α specifies the wavevector projection on the interface between the layer and the outer medium of refractive index $n_a = \sqrt{\varepsilon_a}$ as $\mathbf{k}_{||} = k_0\mathbf{b}$, where $k_0 = \omega/c$ is the vacuum wave number, c is the speed of light in vacuum, and $|\mathbf{b}| = n_a \sin\alpha$. The incidence is illustrated in Fig. 1(a). Due to the translation symmetry in the plane perpendicular to the stratification axis z, the plane-wave solution for the electric field (and similarly for the magnetic field) reads as $\mathbf{E} = \mathbf{E}_0 \exp(ik_0\mathbf{br} + ik_0\eta z - i\omega t)$, where $\mathbf{r}$ is the radius vector and $\eta = k_z/k_0 = n_a \cos\alpha$.

The material parameters are involved into the constitutive equations for the generally bianisotropic and inhomogeneous (stratified) slab:

$$\mathbf{D}(\omega, \mathbf{r}) = \hat{\varepsilon}(\omega, z)\mathbf{E}(\omega, \mathbf{r}) + \hat{\alpha}(\omega, z)\mathbf{H}(\omega, \mathbf{r}),$$
$$\mathbf{B}(\omega, \mathbf{r}) = \hat{\kappa}(\omega, z)\mathbf{E}(\omega, \mathbf{r}) + \hat{\mu}(\omega, z)\mathbf{H}(\omega, \mathbf{r}). \quad (1)$$

Here **D**, **B**, **E**, and **H** are the electric displacement vector, magnetic induction, electric strength, and magnetic strength, respectively, $\hat{\varepsilon}$ is the dielectric permittivity tensor, $\hat{\mu}$ is the magnetic permeability tensor, and $\hat{\alpha}$ and $\hat{\kappa}$ are the gyration pseudotensors.

The approach of homogenization is based on the idea that wave propagation through the stack of layers is equivalent to the wave propagation through a homogeneous effective medium. The effective material parameters are generally more complex than those of the individual slabs and can be both bianisotropic and nonlocal even if the slabs are not.

Plane waves are fully described by the tangential magnetic $\mathbf{H}_t$ and electric $\mathbf{E}_t$ fields lying in the plane (x, y). Further, we discuss the wave solutions of the governing system of equations [41,42], which can be obtained from the Maxwell equations as follows:

$$\frac{d\mathbf{W}}{dz} = ik_0\hat{M}\mathbf{W}, \tag{2}$$

where $\mathbf{W}(z) = (\mathbf{H}_t(z), \mathbf{E}_t(z))^T$ is a multidimensional vector composed of tangential electric and magnetic fields (superscript ^{T} stands for transpose). The matrix $\hat{M}$ depends on the material parameters and can be presented as a block matrix

$$\hat{M} = \begin{pmatrix} A & B \\ C & D \end{pmatrix}, \tag{3}$$

where the matrices A, B, C, and D can be written for arbitrary bianisotropic stratified medium. Since the operator effective medium theory for a stack of planar layers was introduced earlier, we do not show the explicit expressions for these values here, but refer a reader to Ref. [16]. Here, we just outline the fundamentals standing behind the homogenization approach.

It is important that for a homogeneous planar layer, the block matrix $\hat{M}$ is constant. Hence, solution of the differential equation (2) is the product of the matrix exponential $\Omega_{z_0}^z = \exp[ik_0(z-z_0)\hat{M}]$ and "initial" tangential fields $\mathbf{W}(z_0)$ at the plane $z = z_0$:

$$\mathbf{W}(z) = \exp[ik_0(z-z_0)\hat{M}]\mathbf{W}(z_0) = \Omega_{z_0}^z\mathbf{W}(z_0). \tag{4}$$

The propagator $\Omega_{z_0}^z$ describing spatial field propagation is called an evolution operator and is a fundamental solution of the field equations (4). It should be stressed that owing to the electrodynamic boundary conditions the tangential fields $\mathbf{W}(z)$ are continuous across the interfaces between the slabs. That is why for the two slabs of thicknesses d_1 and d_2, one can write $\mathbf{W}(d_1) = \exp[ik_0d_1\hat{M}_1]\mathbf{W}(0)$ and $\mathbf{W}(d_1+d_2) = \exp[ik_0d_2\hat{M}_2]\mathbf{W}(d_1)$ arriving at

$$\mathbf{W}(d_1+d_2) = \exp[ik_0d_2\hat{M}_2]\exp[ik_0d_1\hat{M}_1]\mathbf{W}(0). \tag{5}$$

The evolution operator $\Omega_0^{d_1+d_2} = \Omega_{d_1}^{d_1+d_2}\Omega_0^{d_1}$ of the two-slab system is the product of evolution operators of the individual slabs.

The effective medium is a homogeneous slab with effective material parameters equivalent to the actual inhomogeneous system, e.g., a bilayer. Such a homogeneous slab characterized by the matrix $\hat{M}_{\text{eff}}$ is equivalent to the two-slab system, if evolution operators are indistinguishable, that is,

$$\exp[ik_0(d_1+d_2)\hat{M}_{\text{eff}}] = \exp[ik_0d_2\hat{M}_2]\exp[ik_0d_1\hat{M}_1]. \tag{6}$$

Solution of this equation with respect to $\hat{M}_{\text{eff}}$ is known as the Baker-Campbell-Hausdorff series

$$\begin{aligned}\hat{M}_{\text{eff}} &= \rho_1\hat{M}_1 + \rho_2\hat{M}_2 + \frac{ik_0d}{2}\rho_1\rho_2[\hat{M}_2, \hat{M}_1] \\ &\quad - \frac{(k_0d)^2}{12}\rho_1\rho_2(\rho_1[[\hat{M}_2, \hat{M}_1], \hat{M}_1] \\ &\quad + \rho_2[[\hat{M}_1, \hat{M}_2], \hat{M}_2]) + \cdots,\end{aligned} \tag{7}$$

where $\rho_1 = d_1/d$ and $\rho_2 = d_2/d = 1-\rho_1$ are the volume filling fractions of the materials in the unit cell of thickness $d = d_1 + d_2$ and $[\hat{M}_1, \hat{M}_2]$ is the commutator.

In the limit $k_0d \ll 1$, we can keep only the frequency-independent terms. It is the zeroth-order approximation of the theory allowing us to get the well-known local effective medium parameters

$$\varepsilon_{||} = \rho_1\varepsilon_1 + \rho_2\varepsilon_2, \quad \varepsilon_\perp = \left(\frac{\rho_1}{\varepsilon_1} + \frac{\rho_2}{\varepsilon_2}\right)^{-1} \tag{8}$$

defining the effective permittivity tensor $\hat{\varepsilon} = \text{diag}(\varepsilon_{||}, \varepsilon_{||}, \varepsilon_\perp)$, where ε_1 and ε_2 are the permittivities of the slabs. A higher-order approximation means that one should take into account more terms in the Baker-Campbell-Hausdorff series. These terms depend on the wavevector $\mathbf{k}_{||}$ introducing nonlocality in effective material parameters. This nonlocality implies the importance of the order of layers within a unit cell ignored in the local material parameters Eq. (8).

In Fig. 1(d), we show transmittance of the bilayer and corresponding homogenized system using the local effective medium parameters (8). Due to asymmetry of the system (incident ε_a and exit ε_b media are different), there is a perceptible difference in transmittance through the effective medium compared to that through the bilayer. The difference becomes more pronounced, when the number of layers increases even though the layers are deeply subwavelength [11].

In general, when a medium is continuously inhomogeneous, the matrix $\hat{M}(z)$ is not constant and the evolution operator cannot be presented in the exponential form, but only as a Born series

$$\begin{aligned}\Omega_a^z &= \hat{E} + ik_0\int_a^z dz_1\hat{M}(z_1) \\ &\quad + (ik_0)^2\int_a^z dz_1\hat{M}(z_1)\int_a^{z_1} dz_2\hat{M}(z_2) + \ldots,\end{aligned} \tag{9}$$

where $\hat{E}$ is an identity operator. Both the vector of tangential components $\mathbf{W}$ and matrix $\hat{M}$ can be represented in the four-dimensional space. Then, $\hat{E}$ is the four-dimensional unit matrix.

To derive the effective material parameters of a continuously inhomogeneous layer of thickness $b-a$, we should equate its evolution operator Ω_a^b given by Eq. (9) at $z = b$ to the evolution operator $\exp[ik_0(b-a)\hat{M}_{\text{eff}}]$ of the effectively homogeneous layer. Writing the exponential as a series, we obtain

$$\hat{E} + ik_0(b-a)\hat{M}_{\text{eff}} + \frac{1}{2}(ik_0)^2(b-a)^2\hat{M}_{\text{eff}}^2 + \cdots$$
$$= \hat{E} + ik_0\int_a^b dz_1\hat{M}(z_1) + (ik_0)^2\int_a^b dz_1\hat{M}(z_1)$$
$$\times \int_a^{z_1} dz_2 M(z_2) + \ldots$$

Keeping only the terms up to ik_0 (zeroth-order approximation), we arrive at the effective characteristic matrix

$$\hat{M}_{\text{eff}} = \frac{1}{b-a}\int_a^b dz_1\hat{M}(z_1), \tag{10}$$

providing two components of the effective material tensor as

$$\varepsilon_{||}^{(0)} = \frac{1}{b-a}\int_a^b dz_1\varepsilon(z_1), \quad \varepsilon_{\perp}^{(0)} = \left(\frac{1}{b-a}\int_a^b \frac{dz_1}{\varepsilon(z_1)}\right)^{-1}. \tag{11}$$

For a piecewise-continuous function $\hat{M}(z)$ describing a stack of N slabs, the generalization of the two-slab results is valid,

$$\hat{M}_{\text{eff}} = \sum_{j=1}^{N}\rho_j\hat{M}_j, \tag{12}$$

where ρ_j is the filling fraction of the jth medium. The effective material parameters can be written as follows,

$$\varepsilon_{||}^{(0)} = \sum_{j=1}^{N}\rho_j\varepsilon_j, \quad \varepsilon_{\perp}^{(0)} = \left(\sum_{j=1}^{N}\frac{\rho_j}{\varepsilon_j}\right)^{-1}. \tag{13}$$

As we will see below, spherically and cylindrically symmetric media can be also treated by the operator EMA outlined in this section.

III. OPERATOR EFFECTIVE MEDIUM APPROXIMATION FOR MULTILAYER SPHERICALLY SYMMETRIC SYSTEMS

According to Ref. [43] the spherical coordinates (radial r and angular θ and φ) can be separated for electric and magnetic fields in spherically symmetric bianisotropic media as follows: $\mathbf{E}(\mathbf{r}) = \hat{F}_{lm}(\theta,\varphi)\mathbf{E}(r)$ and $\mathbf{H}(\mathbf{r}) = \hat{F}_{lm}(\theta,\varphi)\mathbf{H}(r)$, where $\hat{F}_{lm}(\theta,\varphi)$ is the tensor function of polar θ and azimuthal φ angles, $l = 1, 2, \ldots,$ and $-l \leqslant m \leqslant l$. By substituting the fields into the Maxwell equations, we obtain the system of ordinary differential equations

$$\frac{d\mathbf{W}}{dr} = ik_0\hat{M}(r)\mathbf{W} \tag{14}$$

for the tangential fields combined to the vector $\mathbf{W}(r) = (\mathbf{H}_t(r), \mathbf{E}_t(r))^T$. The tangential fields are orthogonal to the basis vector of spherical coordinates $\mathbf{e}_r = \mathbf{r}/r$. It is important that in contrast to the planar layers, the matrix $\hat{M}(r)$ depends on the coordinates even for homogeneous spherical layers. The matrix $\hat{M}$ for a rotationally symmetric bianisotropic spherical layer is a block matrix with the components [43]

$$\begin{aligned}
A &= \frac{i}{k_0 r}\hat{I} + \mathbf{e}_r^{\times}\hat{\alpha}\hat{I} - \kappa_{rr}\delta_r\frac{l(l+1)}{k_0^2r^2}\mathbf{e}_\varphi\otimes\mathbf{e}_\theta,\\
B &= \mathbf{e}_r^{\times}\hat{\varepsilon}\hat{I} - \varepsilon_{rr}\delta_r\frac{l(l+1)}{k_0^2r^2}\mathbf{e}_\varphi\otimes\mathbf{e}_\theta,\\
C &= -\mathbf{e}_r^{\times}\hat{\mu}\hat{I} + \mu_{rr}\delta_r\frac{l(l+1)}{k_0^2r^2}\mathbf{e}_\varphi\otimes\mathbf{e}_\theta,\\
D &= \frac{i}{k_0 r}\hat{I} - \mathbf{e}_r^{\times}\hat{\kappa}\hat{I} + \alpha_{rr}\delta_r\frac{l(l+1)}{k_0^2r^2}\mathbf{e}_\varphi\otimes\mathbf{e}_\theta,
\end{aligned} \tag{15}$$

where $\delta_r = (\varepsilon_{rr}\mu_{rr} - \alpha_{rr}\kappa_{rr})^{-1}$ and $\mathbf{e}_\varphi$ and $\mathbf{e}_\theta$ are the basis vectors of the spherical coordinates. We have introduced here a dyad $\mathbf{a}\otimes\mathbf{b}$ and a dual tensor $\mathbf{a}^{\times}$ [41,42,44] with elements a_ib_j and $\varepsilon_{ijk}a_j$, respectively, where ε_{ijk} is the Levi-Civita tensor with indices i, j, and k spanning from 1 to 3. In Eq. (15), we use the dual tensor $\mathbf{e}_r^{\times} = \mathbf{e}_\varphi\otimes\mathbf{e}_\theta - \mathbf{e}_\theta\otimes\mathbf{e}_\varphi$ and the projector $\hat{I} = \mathbf{e}_\theta\otimes\mathbf{e}_\theta + \mathbf{e}_\varphi\otimes\mathbf{e}_\varphi$ on the plane orthogonal to $\mathbf{e}_r$.

In general, the rotationally symmetric material tensors $\hat{\varepsilon}$, $\hat{\mu}$, $\hat{\alpha}$, and $\hat{\kappa}$ can be presented as a sum of three irreducible tensors or, equivalently, as a nondiagonal matrix in the basis $(\mathbf{e}_r, \mathbf{e}_\theta, \mathbf{e}_\varphi)$:

$$\hat{\xi} = \xi_1\mathbf{e}_r\otimes\mathbf{e}_r + \xi_2\hat{I} + i\chi_\xi\mathbf{e}_r^{\times} = \begin{pmatrix} \xi_1 & -i\chi_\xi & 0\\ i\chi_\xi & \xi_2 & 0\\ 0 & 0 & \xi_2\end{pmatrix}, \tag{16}$$

where $\hat{\xi}$ stands for one of the material tensors, while ξ_1 and ξ_2, and χ_ξ are the scalar coefficients.

Solution to the system of differential equations (14) for $\mathbf{W}$ can be formally written by means of the evolution operator Ω_a^r as follows:

$$\mathbf{W}(r) = \Omega_a^r\mathbf{W}(a). \tag{17}$$

Since the matrix $\hat{M}(r)$ depends on the radial coordinate r, the evolution operator is not an exponential. But we can use again the Born series expansion as

$$\Omega_a^r = \hat{E} + ik_0\int_a^r dr_1\hat{M}(r_1)$$
$$+ (ik_0)^2\int_a^r dr_1\hat{M}(r_1)\int_a^{r_1} dr_2M(r_2) + \ldots \tag{18}$$

Here, the identity operator $\hat{E} = \text{diag}(\hat{I}, \hat{I})$ is a block matrix (unit matrix in four-dimensional space). This series is rapidly converging, if $k_0(r-a) \ll 1$, i.e., for subwavelength layers with thicknesses much smaller than radiation wavelength.

Homogenization procedure for a couple of spherical layers stems from the same condition for identity of the bilayer and homogenized layer evolution operators as in the case of planar system:

$$\left(\Omega_a^b\right)_{\text{eff}} = \Omega_c^b\Omega_a^c. \tag{19}$$

Introducing the Born series into this equation, we can write the expressions of different orders, the lowest of which (zeroth order) reads

$$\int_a^b dr\hat{M}_{\text{eff}}(r) = \int_a^c dr\hat{M}_1(r) + \int_c^b dr\hat{M}_2(r). \tag{20}$$

Assuming that the layers to be homogenized are nonmagnetic and isotropic, we can write their A, B, C, and D matrices as

$$A_{1,2} = \frac{i}{k_0 r}\hat{I}, \quad B_{1,2} = \varepsilon_{1,2}\mathbf{e}_r^{\times} - \frac{l(l+1)}{k_0^2 r^2}\mathbf{e}_\varphi \otimes \mathbf{e}_\theta,$$
$$C_{1,2} = -\mathbf{e}_r^{\times} + \frac{l(l+1)}{\varepsilon_{1,2}k_0^2 r^2}\mathbf{e}_\varphi \otimes \mathbf{e}_\theta, \quad D_{1,2} = \frac{i}{k_0 r}\hat{I}. \tag{21}$$

The effective medium of the couple of isotropic spherical layers can be treated as a nonmagnetic anisotropic layer with $\hat{\varepsilon}_{\text{eff}} = \text{diag}(\varepsilon_r, \varepsilon_t, \varepsilon_t)$, the blocks of the matrix $\hat{M}_{\text{eff}}$ being

$$A_{\text{eff}} = \frac{i}{k_0 r}\hat{I}, \quad B_{\text{eff}} = \varepsilon_t\mathbf{e}_r^{\times} - \frac{l(l+1)}{k_0^2 r^2}\mathbf{e}_\varphi \otimes \mathbf{e}_\theta,$$
$$C_{\text{eff}} = -\mathbf{e}_r^{\times} + \frac{l(l+1)}{\varepsilon_r k_0^2 r^2}\mathbf{e}_\varphi \otimes \mathbf{e}_\theta, \quad D_{\text{eff}} = \frac{i}{k_0 r}\hat{I}. \tag{22}$$

Substituting them into the zeroth-order equation (20), we arrive at the pair of equations:

$$\int_a^b \varepsilon_t dr = \int_a^c \varepsilon_1 dr + \int_c^b \varepsilon_2 dr,$$
$$\int_a^b \frac{dr}{\varepsilon_r r^2} = \int_a^c \frac{dr}{\varepsilon_1 r^2} + \int_c^b \frac{dr}{\varepsilon_2 r^2}. \tag{23}$$

Thus the tangential ε_t and radial ε_r components of the effective permittivity tensor read as

$$\varepsilon_t = \rho_1\varepsilon_1 + \rho_2\varepsilon_2, \quad \varepsilon_r = \left(\frac{\rho_1'}{\varepsilon_1} + \frac{\rho_2'}{\varepsilon_2}\right)^{-1}, \tag{24}$$

where $\rho_1 = (c-a)/(b-a)$ and $\rho_2 = (b-c)/(b-a)$ are the radius filling fractions, while $\rho_1' = (c^{-1} - a^{-1})/(b^{-1} - a^{-1})$ and $\rho_2' = (b^{-1} - c^{-1})/(b^{-1} - a^{-1})$ are the curvature filling fractions. The filling fractions obey the equalities $\rho_1 + \rho_2 = 1$ and $\rho_1' + \rho_2' = 1$, being linked through $\rho_1' = (b/c)\rho_1$ and $\rho_2' = (a/c)\rho_2$. In the case of planar layers, the linear filling fractions ρ_1 and ρ_2 coincide with the volume ones, but it is not the case for spherical layers. The curvature filling fractions ρ_1' and ρ_2' use the curvatures $1/R$ of interfaces instead of their radii R, so that they approach ρ_1 and ρ_2, respectively, only when the spherical layers are thin, that is, $a \approx c \approx b$ or $(b-a) \ll c$.

Availability of the curvature filling fractions is a drastic dissimilarity to the planar case resulting in the difference of definitions for the effective permittivity component across the stratification direction. The difference is caused by the curvature of spherical layers, but this fact does not influence locality of the effective permittivity tensor (no dependence on the wave vector). In Fig. 1(f), the scattering efficiency $\sigma_g^{-1}d\sigma/do$ as a differential scattering cross-section normalized by the geometrical cross-section of the particle $\sigma_g = \pi b^2$ is demonstrated, where o denotes the solid angle. We use the scattering theory developed in Ref. [43]. Despite the spherical layers are deeply subwavelength, there is a noticeable gap between the curves for two-shell and homogenized solutions in the range of small scattering angles (forward scattering). This breakdown of the EMA is caused by the total internal reflection due to the great difference between the permittivities of layers.

Except for the scattering diagrams showing how the scattered electromagnetic energy is distributed across the scattering angles θ, the total scattering cross-section σ is a convenient characteristic to estimate efficiency of the homogenization. If the total scattering cross-section of the homogenized system σ_H equals to the total cross-section of the multilayer system, then we can expect good or even perfect homogenization. In Fig. 2(a), we demonstrate the total scattering cross-section of a homogenized system σ_H with respect to the total scattering cross-section of the actual multilayer σ. The plot reveal the importance of the sequence of layers. With the permittivities of the spherical layers $\varepsilon_1 = 2.25$ and $\varepsilon_2 = 4$ the homogenized system is less scattering than the actual mutilayer, whereas for the opposite sequence of layers, $\varepsilon_1 = 4$ and $\varepsilon_2 = 2.25$, the relative scattering σ_H/σ is greater than the unity. Despite the thicknesses of spherical layers are subwavelength ($d \ll \lambda$), the EMA does not work well exhibiting significant deviations of σ_H/σ from 1 for small radii of the core a, i.e., for great curvatures a^{-1}. Thus there is one more criterion for the EMA to be valid: the radii of the layers must not be subwavelength. From Fig. 2(a), we can estimate the minimum core radius as $a_m \approx 100$ nm or, generally, $k_0 a = 2\pi a/\lambda \sim 1$. We can roughly explain such a behavior as follows. When the radius of the core is small ($k_0 a \ll 1$), the inaccuracies of homogenization are well noticed, because the core $c_2 k_0 a$ and layer $c_1 k_0 d$ terms in evolution operator expansion $\hat{\Omega}_a^b \approx \hat{E} + c_1 k_0 d + c_2 k_0 a$ are comparable (here $c_{1,2}$ are constant coefficients). Otherwise, when the core is thick, the effect of subwavelength layers above it can be treated as a small perturbation.

The effective medium approximation can be also validated in the near-field zone, that is, comparing the fields in vicinity of the multilayer and homogenized nanoparticles. Indeed, since the optical force exerting on a particle can be calculated as an integration of the Maxwell stress tensor over any surface embracing the particle, the usage of far fields for EMA validation (through optical force calculation) is equivalent to the usage of near fields. This assumption is confirmed by Fig. 3. In this figure, we can see the far-field (on the left) vs. near-field (on the right) calculations. The ratio of scattering efficiencies across the scattering angles well corresponds to ratio of the near-field intensities.

The components of effective permittivity tensor are shown in Fig. 2(b). Any considered sequence of layers provides the same tangential component ε_t, because it is defined by the thicknesses of layers, i.e., the difference between the layers radii. The situation is fundamentally different for the radial component ε_r which depends on the core radius a itself, see Eq. (24). Dependence on the radius disappears for ε_r calculated in the framework of the planar effective medium theory with Eq. (8), see the dash-dotted line in Fig. 2(b). In this case, as we observe in Fig. 2(a), the ratio of scattering cross-sections follows the curve for spherical EMA starting from about 100 nm. Thus one can exploit the planar effective medium theory as a proxy for the spherical EMA in the range of its validity.

Now turn to the metal-dielectric spherical nanoparticles. When the magnitude of metal permittivity is large, $|\varepsilon_2| > \varepsilon_1$

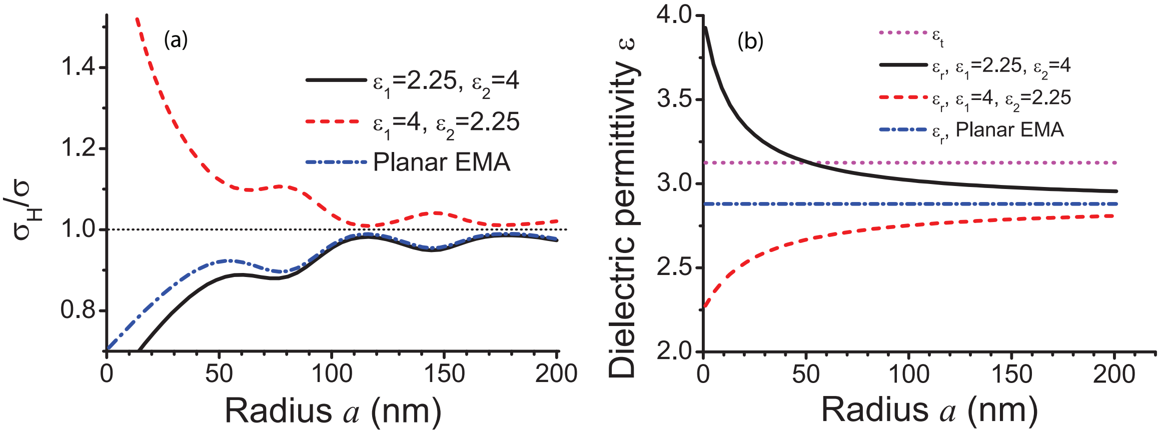

FIG. 2. (a) Ratio of total scattering cross-sections of homogenized σ_H and actual σ multilayer dielectric systems in the case of two sequences of layers. The planar effective medium parameters are shown for comparison as well. (b) Permittivities of the effective medium tensor components ε_t and ε_r. Parameters for calculation: $\varepsilon_a = 1$, $\varepsilon_b = 2$, thicknesses of layers are $d_1 = d_2 = 20$ nm, and wavelength $\lambda = 500$ nm.

as in Fig. 4(a), the dependence on the core radius a becomes intricate. The range of validity of the spherical EMA shifts to larger radii and the estimation $k_0 a \sim 1$ is not valid anymore. So, we need to have core radii of around a wavelength or greater or, in other words, the curvature of the core should be confined within the inverse wavelength as

$$a^{-1} < \lambda^{-1}. \tag{25}$$

As shown in Fig. 4(b), the permittivity component ε_r has a pole associated with vanishing of its denominator at $a \approx 50$ nm where $\varepsilon_1 \rho_2' + \varepsilon_2 \rho_1' = 0$. So, we can distinguish the range of anisotropic metallic and hyperbolic regimes below and above the pole. Notice that poles in permittivities in Figs. 4(b) and (d) do not guarantee existence of a scattering zero. Applying the planar EMA for calculation of the effective material parameters, we arrive at an effective hyperbolic medium with no dependence on the radius a.

If $|\varepsilon_2| < \varepsilon_1$, then the ratio of total scattering cross-sections is mostly a monotonic function, as shown in Fig. 4(c). The total scattering cross-section ratio for planar and spherical EMA are quite close from about $a = 100$ nm. All in all, the EMA operates worse for metal-containing than for all-dielectric systems.

The effective medium theory does not put restrictions on the imaginary part of the permittivity. In Fig. 5, we vary the imaginary part in a wide range of values including both positive (loss) and negative (gain) ones. We do not observe noticeable change in the ratio of total cross-sections of homogenized and multilayer systems.

As another option, we can try to include a core to the proposed homogenization procedure. To this end, we

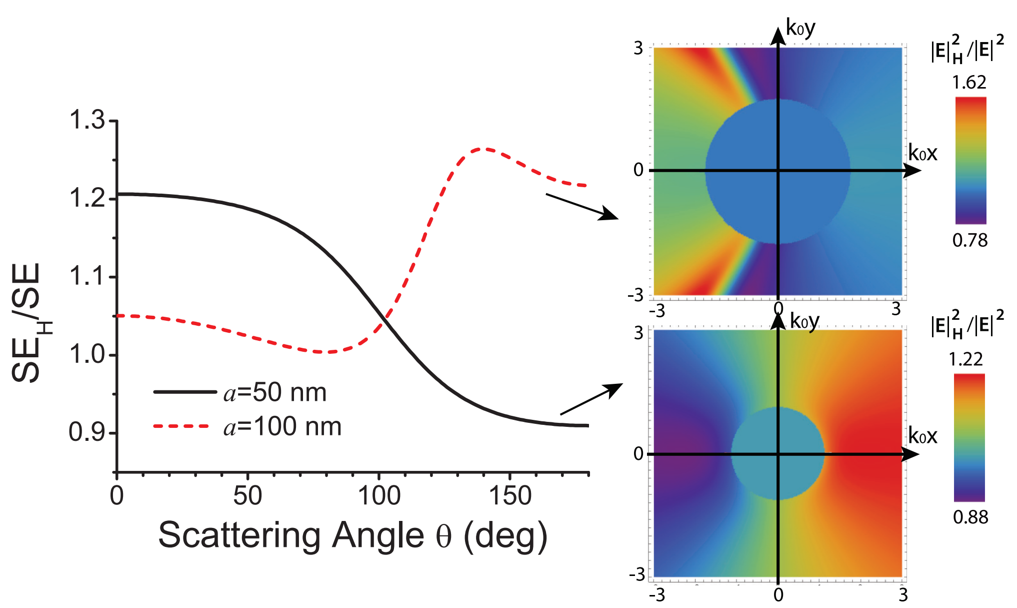

FIG. 3. Ratio of scattering efficiencies for homogenized SE_H and multilayer SE systems. The ratio of the scattered field intensities in the near field is shown on the right. Parameters for calculation: $\varepsilon_a = 1$, $\varepsilon_b = 2$, $\varepsilon_1 = 4$, $\varepsilon_2 = 2.25$, thicknesses of layers are $d_1 = d_2 = 20$ nm, and wavelength $\lambda = 500$ nm.

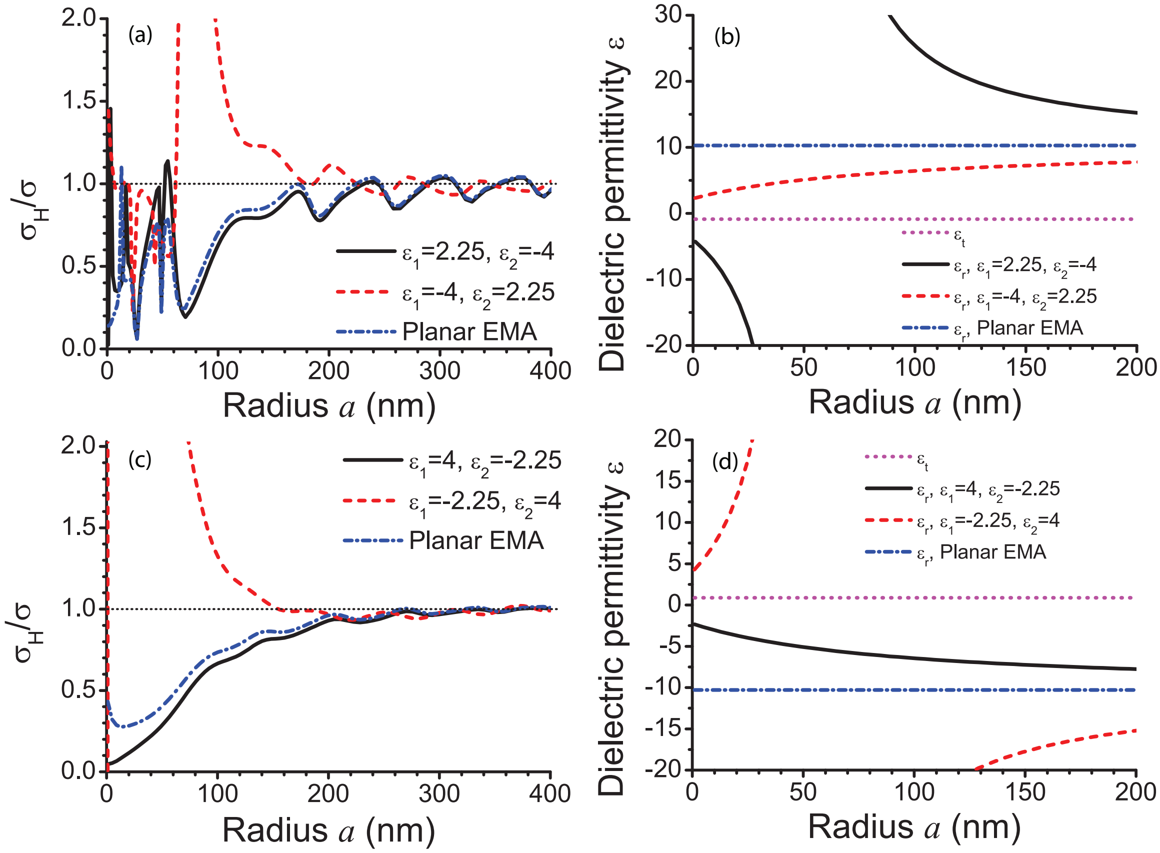

FIG. 4. [(a) and (c)] Ratio of total scattering cross-sections of homogenized σ_H and actual σ multilayer metal-dielectric systems. Homogenization is performed both using spherical and planar effective medium parameters. [(b) and (d)] Dielectric permittivities of the effective medium tensor components ε_t and ε_r. Parameters for calculation: $\varepsilon_a = 1$, $\varepsilon_b = 2$, thicknesses of layers are $d_1 = d_2 = 20$ nm, and wavelength $\lambda = 500$ nm.

formally divide the inner region with refractive index ε_b into a small core of radius $a_0 \ll a$ and a thick layer $a_0 < r < a$, both of the same permittivity ε_b. Then, we are able to homogenize three layers assuming that the contribution of the small core is negligible. As a result,

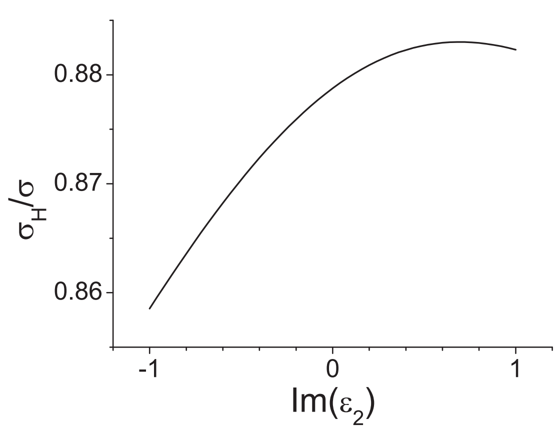

FIG. 5. Ratio of total scattering cross-sections for homogenized σ_H and multilayer σ systems vs. imaginary part of the dielectric permittivity $\mathrm{Im}(\varepsilon_2)$. Parameters for calculation: $\varepsilon_a = 1$, $\varepsilon_b = 2$, $\mathrm{Re}(\varepsilon_1) = 4$, $\varepsilon_2 = 2.25$, radius of the core $a = 50$ nm, thicknesses of layers are $d_1 = d_2 = 20$ nm, and wavelength $\lambda = 500$ nm.

we get the effective medium parameters of the spherical nanoparticle

$$\varepsilon_t = \rho_1\varepsilon_1 + \rho_2\varepsilon_2 + \rho_b\varepsilon_b, \quad \varepsilon_r = \left(\frac{\rho_1'}{\varepsilon_1} + \frac{\rho_2'}{\varepsilon_2} + \frac{\rho_b'}{\varepsilon_b}\right)^{-1}, \tag{26}$$

where $\rho_1 = (c-a)/(b-a_0)$, $\rho_2 = (b-c)/(b-a_0)$, $\rho_b = (a-a_0)/(b-a_0)$, $\rho_1' = (c^{-1}-a^{-1})/(b^{-1}-a_0^{-1})$, $\rho_2' = (b^{-1}-c^{-1})/(b^{-1}-a_0^{-1})$, and $\rho_b' = (a^{-1}-a_0^{-1})/(b^{-1}-a_0^{-1})$. Since $a_0 \ll a$, the radius and curvature filling fractions can be recast as $\rho_1 \approx (c-a)/b$, $\rho_2 \approx (b-c)/b$, $\rho_b \approx a/b$, $\rho_1' \approx 0$, $\rho_2' \approx 0$, and $\rho_b' \approx 1$, so that the material parameters of the homogenized anisotropic particle corresponding to the whole spherical multilayer read as

$$\varepsilon_t = \frac{c-a}{b}\varepsilon_1 + \frac{b-c}{b}\varepsilon_2 + \frac{a}{b}\varepsilon_b, \quad \varepsilon_r = \varepsilon_b. \tag{27}$$

The tangential effective permittivity ε_t represents just a mixing rule, while the radial permittivity ε_r is defined solely by the core permittivity. As clearly seen from Fig. 6(a) in comparison to Fig. 1(f), the inclusion of the core to the homogenization procedure does not improve accuracy of the effective-medium theory, but only worsen it. The reason is the high curvature of the inner boundary of the core layer a_0^{-1}. We can obtain the better scattering pattern for some radii a. As

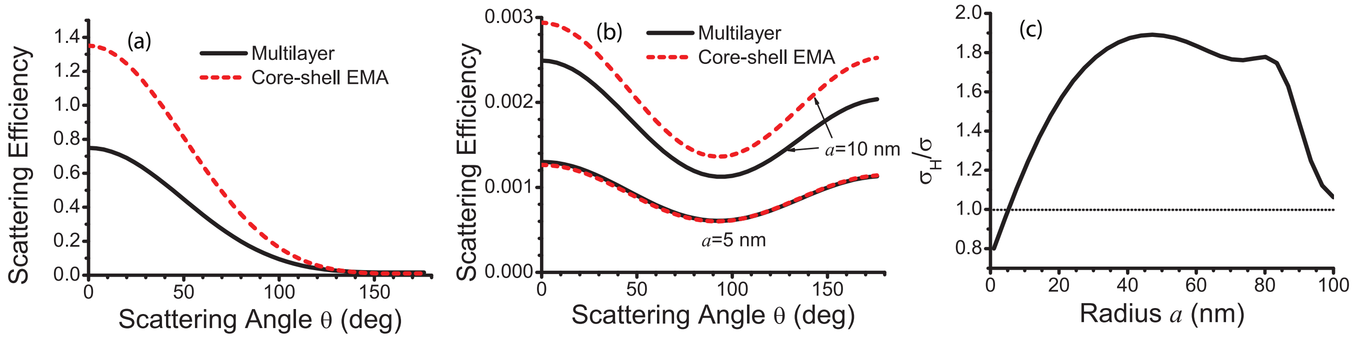

FIG. 6. Homogenization of the whole particle including both core and shell for core radii (a) $a = \lambda/2\pi$ and (b) $a = 5$ and 10 nm. (c) Ratio of total scattering cross-sections of homogenized σ_H and multilayer σ systems. Parameters: $\varepsilon_1 = 1$, $\varepsilon_2 = 5$, $\varepsilon_a = 1$, $\varepsilon_b = 5$, thicknesses of layers are $d_1 = d_2 = 10$ nm, and wavelength $\lambda = 500$ nm.

demonstrated in Fig. 6(b), the scattering efficiency curves for homogenized and actual structures get closer for $a = 10$ nm and may even almost coincide for $a = 5$ nm. We explain such a behavior by the compromise between the two criteria for EMA validity. On the one hand, the smaller thickness of the layer, the better. On the other hand, the small radius (great curvature) brings us to the breakdown of the homogenization. When these two effects are compensated, the homogenization is perfect. According to Fig. 6(c) the value $a \approx 5$ nm is an optimal value for the EMA. Optimal values can be found for greater radii a as well representing a set of discrete accidental values. Nevertheless, optimization of the total scattering does not mean that the distributions across the scattering angles coincide for multilayer and homogenized particles. The distribution may be the same for electric dipole particles, but the scattering patterns for bigger particles are defined by the interplay of multipoles causing their ambiguity. Thus the core cannot be reliably included into our homogenization scheme.

IV. OPERATOR EFFECTIVE MEDIUM APPROXIMATION FOR MULTILAYER CYLINDRICALLY SYMMETRIC SYSTEMS

In this section, we consider propagation of electromagnetic waves in cylindrically symmetric bianisotropic media described by the material tensors $\hat{\xi} = \{\hat{\varepsilon}, \hat{\mu}, \hat{\alpha}, \hat{\kappa}\}$ given by

$$\hat{\xi} = \sum_{i,j=1}^{3} \xi_{ij}(r)\mathbf{e}_i \otimes \mathbf{e}_j, \tag{28}$$

where $\mathbf{e}_1 = \mathbf{e}_r$, $\mathbf{e}_2 = \mathbf{e}_\varphi$, and $\mathbf{e}_3 = \mathbf{e}_z$ are the basis vectors of the cylindrical coordinates (r, φ, z). Due to the azimuthal and translational symmetries available for waves in cylindrically symmetric media, we can write the magnetic and electric fields as

$$\begin{pmatrix}\mathbf{H}(\mathbf{r})\\ \mathbf{E}(\mathbf{r})\end{pmatrix} = \exp(i\beta z + i\nu\varphi)\begin{pmatrix}\mathbf{H}(r)\\ \mathbf{E}(r)\end{pmatrix}, \tag{29}$$

where $\beta = k_z$ is the z projection of the wave vector and ν is an integer number. Both β and ν describe the wave vector in the plane orthogonal to the stratification direction r.

As well as for spherically symmetric stratified media, the cylindrical waves satisfy the system of ordinary differential equations (14) for tangential electric and magnetic fields $\mathbf{W} = (\mathbf{H}_t, \mathbf{E}_t)^T$ with the blocks of the matrix $\hat{M}$ given below [45]:

$$A = \frac{i}{k_0 r}\mathbf{e}_\varphi \otimes \mathbf{e}_\varphi + \mathbf{e}_r^\times \hat{\alpha}\hat{I} + \mathbf{e}_r^\times \hat{\varepsilon}\mathbf{e}_r \otimes \mathbf{v}_3 + \mathbf{e}_r^\times(\mathbf{u} + \hat{\alpha}\mathbf{e}_r) \otimes \mathbf{v}_1,$$
$$B = \mathbf{e}_r^\times \hat{\varepsilon}\hat{I} + \mathbf{e}_r^\times \hat{\varepsilon}\mathbf{e}_r \otimes \mathbf{v}_4 + \mathbf{e}_r^\times(\mathbf{u} + \hat{\alpha}\mathbf{e}_r) \otimes \mathbf{v}_2,$$
$$C = -\mathbf{e}_r^\times \hat{\mu}\hat{I} - \mathbf{e}_r^\times \hat{\mu}\mathbf{e}_r \otimes \mathbf{v}_1 + \mathbf{e}_r^\times(\mathbf{u} - \hat{\kappa}\mathbf{e}_r) \otimes \mathbf{v}_3,$$
$$D = \frac{i}{k_0 r}\mathbf{e}_\varphi \otimes \mathbf{e}_\varphi - \mathbf{e}_r^\times \hat{\kappa}\hat{I} - \mathbf{e}_r^\times \hat{\mu}\mathbf{e}_r \otimes \mathbf{v}_2 + \mathbf{e}_r^\times(\mathbf{u} - \hat{\kappa}\mathbf{e}_r) \otimes \mathbf{v}_4,$$

where $\hat{I} = \mathbf{e}_\varphi \otimes \mathbf{e}_\varphi + \mathbf{e}_z \otimes \mathbf{e}_z$ is the projection operator on the surface orthogonal to $\mathbf{e}_r$,

$$\mathbf{v}_1 = \delta_r(\kappa_{rr}\mathbf{e}_r\hat{\alpha}\hat{I} - \varepsilon_{rr}\mathbf{e}_r\hat{\mu}\hat{I} - \kappa_{rr}\mathbf{u}),$$
$$\mathbf{v}_2 = \delta_r(\kappa_{rr}\mathbf{e}_r\hat{\varepsilon}\hat{I} - \varepsilon_{rr}\mathbf{e}_r\hat{\kappa}\hat{I} - \varepsilon_{rr}\mathbf{u})$$
$$\mathbf{v}_3 = \delta_r(\alpha_{rr}\mathbf{e}_r\hat{\mu}\hat{I} - \mu_{rr}\mathbf{e}_r\hat{\alpha}\hat{I} + \mu_{rr}\mathbf{u}),$$
$$\mathbf{v}_4 = \delta_r(\alpha_{rr}\mathbf{e}_r\hat{\kappa}\hat{I} - \mu_r\mathbf{e}_r\hat{\varepsilon}\hat{I} + \alpha_{rr}\mathbf{u}),$$
$$\mathbf{u} = \frac{\beta}{k_0}\mathbf{e}_\varphi - \frac{\nu}{k_0 r}\mathbf{e}_z, \quad \delta_r = (\varepsilon_{rr}\mu_{rr} - \alpha_{rr}\kappa_{rr})^{-1}.$$

Similar to the case of spherical symmetry, the matrix $\hat{M}$ depends on r even for homogeneous media. That is why the evolution operator Ω_a^r can be again presented in the form of the Born series Eq. (18). Looking for the effective medium as a nonmagnetic anisotropic one with the permittivity tensor $\hat{\varepsilon}_{\text{eff}} = \text{diag}(\varepsilon_r, \varepsilon_t, \varepsilon_t)$ and introducing the corresponding matrices A, B, C, and D for isotropic and effective anisotropic cylindrical layers into Eq. (20), one obtains a system of equations for two constant components ε_t and ε_r of the effective permittivity tensor as

$$\int_a^b \varepsilon_t dr = \int_a^c \varepsilon_1 dr + \int_c^b \varepsilon_2 dr,$$
$$\int_a^b \frac{\mathbf{e}_r^\times \mathbf{u} \otimes \mathbf{u}}{\varepsilon_r} dr = \int_a^c \frac{\mathbf{e}_r^\times \mathbf{u} \otimes \mathbf{u}}{\varepsilon_1} dr + \int_c^b \frac{\mathbf{e}_r^\times \mathbf{u} \otimes \mathbf{u}}{\varepsilon_2} dr. \tag{30}$$

The second of these equations is generally a system of four equations, whereas we have only two variables ε_t and ε_r. Therefore the initial ansatz of the nonmagnetic uniaxial effective medium with the z-oriented optical axis exploited for spherically symmetric and planar cases is not applicable

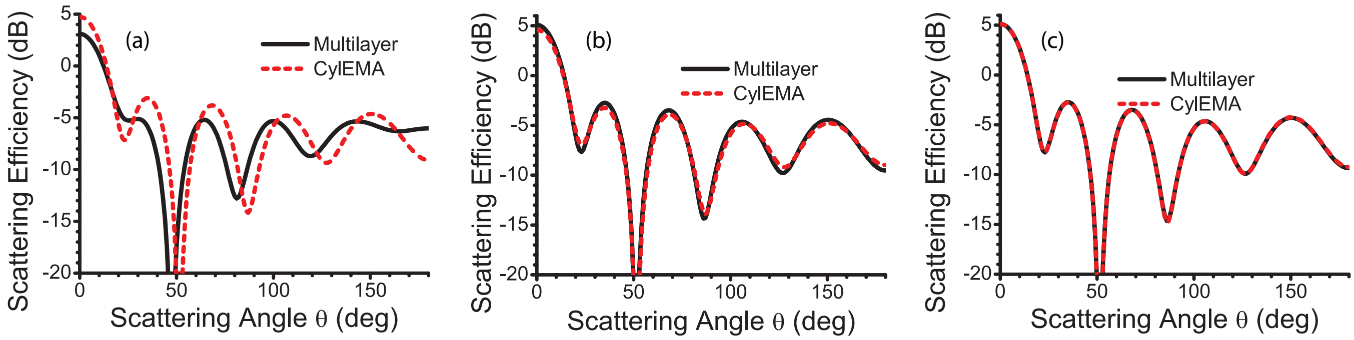

FIG. 7. Scattering efficiency of the periodic multilayer and homogenized systems for the number of periods (a) $N_p = 1$, (b) 5, and (c) 10 between the core of radius $k_0a = 4$ and the outer radius $k_0b = 5.25$. Parameters: permittivities of materials in a unit cell $\varepsilon_1 = 2.25$ and $\varepsilon_2 = 12.25$, $\varepsilon_a = 1$, $\varepsilon_b = -2$.

here. Five equations (30) can be consistently solved for five effective material parameters. Since the effective material tensors are not unique, we can assume a specific form for them, for example,

$$\hat{\varepsilon}_{\text{eff}} = \mathbf{e}_r \otimes \mathbf{e}_r + \varepsilon_t \hat{I},$$
$$\hat{\mu}_{\text{eff}} = \mathbf{e}_r \otimes \mathbf{e}_r + \mu_{\varphi\varphi}\mathbf{e}_\varphi \otimes \mathbf{e}_\varphi + \mu_{\varphi z}\mathbf{e}_\varphi \otimes \mathbf{e}_z + \mu_{z\varphi}\mathbf{e}_z \otimes \mathbf{e}_\varphi + \mu_{zz}\mathbf{e}_z \otimes \mathbf{e}_z, \quad (31)$$

implying that the effective medium is magnetic and anisotropic. Then, the effective parameters sought for can be determined from equations similar to Eq. (30):

$$\int_a^b \varepsilon_t dr = \int_a^c \varepsilon_1 dr + \int_c^b \varepsilon_2 dr,$$
$$\int_a^b C_{\text{eff}}(r) dr = \int_a^c C_1(r) dr + \int_c^b C_2(r) dr, \quad (32)$$

where we have introduced the corresponding block of matrix $\hat{M}_{\text{eff}}$,

$$C_{\text{eff}}(r) = -\mathbf{e}_r^\times \hat{\mu}_{\text{eff}} \hat{I} + \mathbf{e}_r^\times \mathbf{u} \otimes \mathbf{u}. \quad (33)$$

Substituting $\hat{\mu}_{\text{eff}}$ and $\mathbf{u}$ into C_{eff} and using $C_{1,2} = -\mathbf{e}_r^\times + \varepsilon_{1,2}^{-1}\mathbf{e}_r^\times \mathbf{u} \otimes \mathbf{u}$, we arrive at the effective-medium parameters

$$\varepsilon_t = \varepsilon_1\rho_1 + \varepsilon_2\rho_2, \quad \mu_{\varphi\varphi} = 1 + \eta_1 \frac{\beta^2}{k_0^2},$$
$$\mu_{zz} = 1 + \eta_2 \frac{\nu^2}{k_0^2 ab}, \quad \mu_{\varphi z} = \mu_{z\varphi} = \eta_3 \frac{\beta\nu}{k_0^2(b-a)}, \quad (34)$$

where

$$\eta_1 = 1 - \frac{\rho_1}{\varepsilon_1} - \frac{\rho_2}{\varepsilon_2}, \quad \eta_2 = 1 - \frac{\rho_1'}{\varepsilon_1} - \frac{\rho_2'}{\varepsilon_2},$$
$$\eta_3 = \frac{1}{\varepsilon_1} \ln\left(\frac{c}{a}\right) + \frac{1}{\varepsilon_2} \ln\left(\frac{b}{c}\right) - \ln\left(\frac{b}{a}\right). \quad (35)$$

The derived effective material parameters exhibit dependence on the wavevector through β and ν, i.e., this material is nonlocal. For $\beta = 0$ and any ν, there is no wave propagation along the z-axis and the effective permeability is reduced to $\hat{\mu}_{\text{eff}} = \mathbf{e}_r \otimes \mathbf{e}_r + \mathbf{e}_\varphi \otimes \mathbf{e}_\varphi + \mu_{zz}\mathbf{e}_z \otimes \mathbf{e}_z$. The diagonal permeability $\hat{\mu}_{\text{eff}} = \mathbf{e}_r \otimes \mathbf{e}_r + \mu_{\varphi\varphi}\mathbf{e}_\varphi \otimes \mathbf{e}_\varphi + \mathbf{e}_z \otimes \mathbf{e}_z$ occurs for $\nu = 0$ and $\beta \neq 0$.

Some specific situations can be revealed in terms of effective permittivity tensor $\hat{\varepsilon}_{\text{eff}}$ at $\mu_{\text{eff}} = 1$. When $\nu = 0$, the vector $\mathbf{u} = (\beta/k_0)\mathbf{e}_\varphi$ and only two effective parameters ε_t and ε_r determined from Eq. (30) are needed. In this case, we obtain the parameters coinciding with those for the homogenized planar slabs given by Eq. (8). These effective parameters correspond to fiber's fundamental modes. When $\beta = 0$ (wave scattering in cylinder's cross-section), the vector $\mathbf{u} = -(\nu/k_0 r)\mathbf{e}_z$ depends on the radial coordinate bringing us to the effective medium parameters coinciding with those for the spherically symmetric layers given by Eq. (24). Curiously, the effective material parameters for $\beta = 0$ and for $\nu = 0$ are local, when we exploit anisotropic nonmagnetic medium ansatz, and nonlocal for anisotropic magnetic effective media.

Further, we consider some numerical examples related to the EMA in the cross-section of the cylindrical particle, i.e., for $\beta = 0$. We use the scattering theory described in Ref. [46]. Figure 7 deals with the nonmagnetic ansatz for the effective medium described by the dielectric permittivity tensor $\hat{\varepsilon}_{\text{eff}} = \varepsilon_r\mathbf{e}_r \otimes \mathbf{e}_r + \varepsilon_t\hat{I}$. We explore the effect of layer number on the performance of homogenization approach. To this end, we divide the region between the fixed core radius a and fixed outer radius b into different numbers of equal-thickness layers. We assume that N_p periods can be placed within the range $a \leqslant r \leqslant b$, a period being composed of two materials ε_1 and ε_2 and having the thickness $(b-a)/N_p$. In our example, the core is metallic with $\varepsilon_b = -2$. If permittivities of layers are ε_i and their radial and curvature filling fractions are respectively ρ_i and ρ_i', then the effective permittivities read

$$\varepsilon_t = \sum_{i=1}^{2N_p} \rho_i \varepsilon_i, \quad \varepsilon_r = \left(\sum_{i=1}^{2N_p} \frac{\rho_i'}{\varepsilon_i}\right)^{-1}. \quad (36)$$

When the shell is divided only into two homogeneous regions, there is a rough similarity between the scattering efficiency lines for the multilayer and cylindrical effective medium as seen in Fig. 7(a). The lines get closer for the greater number of periods [see Fig. 7(b)] resulting in the perfect correspondence in Fig. 7(c). This behavior can be understood as follows. If we divide the shell into the larger number of periods, then each of the layers becomes thinner (more subwavelength) improving accuracy of the effective medium description. When we decrease the core radius a, the curvature effect cannot be neglected and the scattering efficiency using the cylindrical EMA departures from that for actual multilayer.

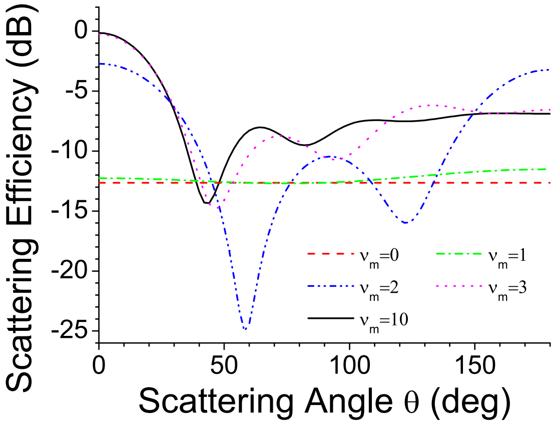

FIG. 8. Scattering efficiency of the homogenized ten-period multilayer system when ν_m partial cylindrical waves are accounted for. Parameters: $k_0a = 4$, $k_0b = 5.25$, $\varepsilon_1 = 0.54$, $\varepsilon_2 = 7.46$, $\varepsilon_a = 1$, and $\varepsilon_b = -2$.

To have a similar scattering pattern, the multilayer and homogenized system should possess the same set of multipoles contributing with T_ν to the scattering efficiency. In Fig. 8, one can see the scattering efficiencies $\sigma_g^{-1} d\sigma/do = \sum_{\nu=-\nu_m}^{\nu_m} T_\nu$, when we truncate the multipole series with number ν_m. Only for $\nu_m = 3$ we get the curve resembling the actual scattering efficiency (solid curve).

According to the discussion above, the second set of effective material parameters to homogenize a cylindrical shell for $\beta = 0$ corresponds to a magnetic nonlocal effective medium described with

$$\begin{aligned}\hat{\varepsilon}_{\text{eff}} &= \mathbf{e}_r \otimes \mathbf{e}_r + (\varepsilon_1\rho_1 + \varepsilon_2\rho_2)\hat{I},\\ \hat{\mu}_{\text{eff}} &= \mathbf{e}_r \otimes \mathbf{e}_r + \mathbf{e}_\varphi \otimes \mathbf{e}_\varphi\\ &\quad + \left[1 + \left(1 - \frac{\rho_1'}{\varepsilon_1} - \frac{\rho_2'}{\varepsilon_2}\right)\right]\frac{\nu^2}{k_0^2 ab}\mathbf{e}_z \otimes \mathbf{e}_z. \qquad (37)\end{aligned}$$

Here we pose a question: whether nonmagnetic and magnetic EMAs are equivalent? If not, then which one better describes a multilayer? Figure 7 helps us to answer these questions. We clearly see that the two EMAs are not equivalent. It is possible that there is an optimal EMA or each EMA has a certain region of parameters where it operates better. To explore these possibilities, a separate investigation is needed. Here, we just compare the two sets of effective medium parameters depending on the core radius a. For deeply subwavelength cores as in Fig. 9(a), the difference between the scattering cross-sections for magnetic and nonmagnetic EMAs is great in the whole range of scattering angles θ, the nonmagnetic EMA describes the multilayer much better. At $a = 50$ nm [Fig. 9(b)], the scattering efficiency curve for magnetic EMA is closer to the curve for actual multilayer for small scattering angles, but overall the two approximations have roughly the same performance. For even bigger particles as in Fig. 9(c), the nonmagnetic EMA again outperforms the magnetic one. In general, the nonmagnetic EMA (with the vacuum magnetic permeability and local dielectric permittivity) operates better than its magnetic counterpart. Nonlocality could further help to improve the homogenization theory by adding more corrections beyond the available local EMA [31].

V. FIRST-ORDER EFFECTIVE MEDIUM APPROXIMATION FOR CYLINDRICALLY SYMMETRIC MEDIA

In this section, we reveal a technique for determining higher-order approximations of effective medium theory considering a cylindrically symmetric system as an example. Similar approach is applicable for spherically symmetric systems as well. In order to find the first-order approximation, we should account for the terms up to $(ik_0)^2$ in the Born expansions for effective medium and individual layers. Then, the equality of evolution operators in the first-order approximation reads

$$\begin{aligned}&\int_a^b dr_1 \hat{M}_{\text{eff}}(r_1) + ik_0 \int_a^b dr_1 \hat{M}_{\text{eff}}(r_1) \int_a^{r_1} dr_2 \hat{M}_{\text{eff}}(r_2)\\ &\quad = \int_a^c dr_1 \hat{M}_1(r_1) + ik_0 \int_a^c dr_1 \hat{M}_1(r_1) \int_a^{r_1} dr_2 \hat{M}_1(r_2)\\ &\qquad + \int_c^b dr_1 \hat{M}_2(r_1) + ik_0 \int_c^b dr_1 \hat{M}_2(r_1) \int_c^{r_1} dr_2 \hat{M}_2(r_2)\\ &\qquad + ik_0 \int_c^b dr_1 \hat{M}_2(r_1) \int_a^c dr_1 \hat{M}_1(r_1). \qquad (38)\end{aligned}$$

The block matrix of the effective medium can be also expanded with respect to the powers of ik_0 as $\hat{M}_{\text{eff}} = \hat{M}_{\text{eff}}^{(0)} + ik_0 \hat{M}_{\text{eff}}^{(1)}$, where $\hat{M}_{\text{eff}}^{(0)}$ is the zeroth-order

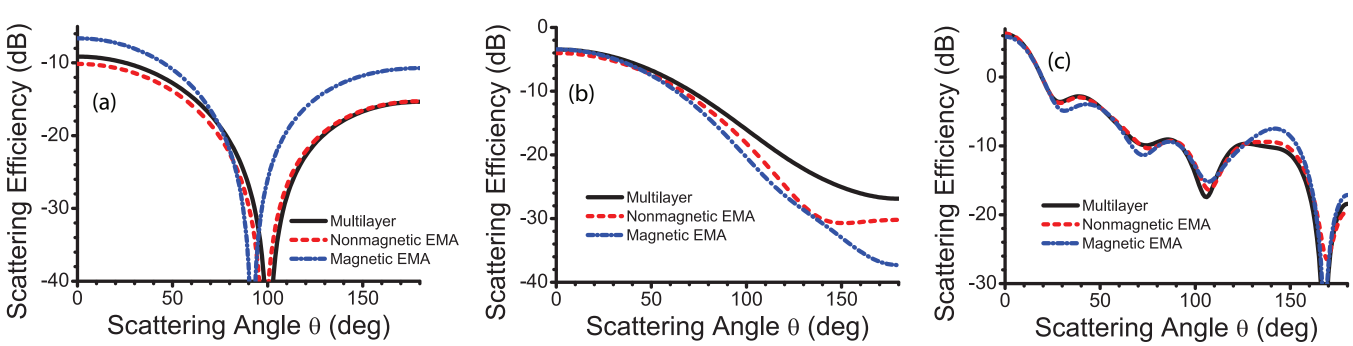

FIG. 9. Scattering efficiency of the two-shell cylindrical particle and corresponding nonmagnetic and magnetic homogenized systems for core radii (a) $a = 20$, (b) 50, and (c) 400 nm. Parameters: thicknesses of layers $d_1 = d_2 = 20$ nm, $\lambda = 500$ nm, $\varepsilon_1 = 2.25$, $\varepsilon_2 = 4$, $\varepsilon_a = 1$, and $\varepsilon_b = 2$.

approximation discussed earlier and defined in Eq. (20). Since the second term on the left-hand side of Eq. (38) is the first-order term, as a first iteration, we can substitute the zeroth-order matrix $\hat{M}_{\rm eff}^{(0)}$ in the integrands there. Thus the effective-medium parameters with contributions of both the zeroth- and first-order terms can be extracted from the matrix $\hat{M}_{\rm eff}$ defined as

$$\begin{aligned}\int_a^b dr_1\hat{M}_{\rm eff}(r_1) = &- ik_0\int_a^b dr_1\hat{M}_{\rm eff}^{(0)}(r_1)\int_a^{r_1} dr_2\hat{M}_{\rm eff}^{(0)}(r_2)\\ &+\int_a^c dr_1\hat{M}_1(r_1)+ik_0\int_a^c dr_1\hat{M}_1(r_1)\\ &\times\int_a^{r_1} dr_2\hat{M}_1(r_2)\\ &+\int_c^b dr_1\hat{M}_2(r_1)+ik_0\int_c^b dr_1\hat{M}_2(r_1)\\ &\times\int_c^{r_1} dr_2\hat{M}_2(r_2)\\ &+ik_0\int_c^b dr_1\hat{M}_2(r_1)\int_a^c dr_1\hat{M}_1(r_1).\end{aligned}\tag{39}$$

For isotropic nonmagnetic cylindrical layers, we know the matrices $\hat{M}_1$, $\hat{M}_2$, and $\hat{M}_{\rm eff}^{(0)}$ involved in the right-hand side of Eq. (39). Introducing them to Eq. (39), we can find the effective permittivity and permeability tensors (and gyration tensors $\hat{\alpha}_{\rm eff}$ and $\hat{\kappa}_{\rm eff}$, if necessary). In the specific case of $\beta = 0$, the effective-medium tensors can be chosen as

$$\begin{aligned}\hat{\varepsilon}_{\rm eff} &= \mathbf{e}_r\otimes\mathbf{e}_r+\varepsilon_{r\varphi}\mathbf{e}_r\otimes\mathbf{e}_\varphi+\varepsilon_{\varphi r}\mathbf{e}_\varphi\otimes\mathbf{e}_r+\varepsilon_{\varphi\varphi}\mathbf{e}_\varphi\otimes\mathbf{e}_\varphi\\ &\quad+\varepsilon_{zz}\mathbf{e}_z\otimes\mathbf{e}_z,\\ \hat{\mu}_{\rm eff} &= \mathbf{e}_r\otimes\mathbf{e}_r+\mu_{r\varphi}\mathbf{e}_r\otimes\mathbf{e}_\varphi+\mu_{\varphi r}\mathbf{e}_\varphi\otimes\mathbf{e}_r+\mu_{\varphi\varphi}\mathbf{e}_\varphi\otimes\mathbf{e}_\varphi\\ &\quad+\mu_{zz}\mathbf{e}_z\otimes\mathbf{e}_z,\end{aligned}\tag{40}$$

The material parameters in the first-order approximation are spatially dispersive and cumbersome. Moreover, the effective tensors contain nondiagonal terms and, thus, it is not a simple task to find the solution of the Maxwell equations with these material parameters. So, as long as it is possible, it is reasonable in practice to limit analysis to the zeroth-order approximation.

VI. BALANCING LOSS AND GAIN

In this section, we show how to leverage effective material parameters for balancing loss and gain in multilayer systems of different geometries. We assume two layers with complex permittivities $\varepsilon_1 = \varepsilon_1' + i\varepsilon_1''$ and $\varepsilon_2 = \varepsilon_2' + i\varepsilon_2''$ and suppose that loss and gain are balanced, when the effective material parameters are real-valued, i.e., there is no net amplification or attenuation of waves propagating through such an effective medium. For the spherical bilayers, for example, this condition means

$$\varepsilon_t = \varepsilon_t^*,\quad \varepsilon_r = \varepsilon_r^*.\tag{41}$$

or

$$\mathrm{Im}(\varepsilon_t) = 0,\quad \mathrm{Im}(\varepsilon_r) = 0.\tag{42}$$

Using Eq. (24), we can rewrite these equations as

$$\begin{aligned}\rho_1\varepsilon_1''+\rho_2\varepsilon_2'' &= 0,\\ \rho_1'\varepsilon_1''|\varepsilon_2|^2+\rho_2'\varepsilon_2''|\varepsilon_1|^2 &= 0.\end{aligned}\tag{43}$$

It is seen that the imaginary parts of permittivities should have different signs to compensate absorption in the passive medium ($\varepsilon'' > 0$) with amplification in the active medium ($\varepsilon'' < 0$).

Planar bilayer. In this case, since the layers are not curved, we should exploit ρ_1 and ρ_2 instead of ρ_1' and ρ_2', respectively, in Eq. (43) [compare Eqs. (24) and (8)]. This means that the absolute values of permittivities should be equal, $|\varepsilon_1|^2 = |\varepsilon_2|^2$, while the imaginary parts should be related as $\varepsilon_2'' = -\rho_1\varepsilon_1''/\rho_2$. The former condition provides the relationship between the real and imaginary parts of permittivities strongly restricting fabrication capabilities of such structures. Therefore it is reasonable to assume that ε' and ε'' are independent and write the conditions for them separately as $\varepsilon_1'^2 = \varepsilon_2'^2$ and $\varepsilon_1''^2 = \varepsilon_2''^2$ instead of $|\varepsilon_1|^2 = |\varepsilon_2|^2$. Since ε_1'' and ε_2'' have opposite signs, we have $\varepsilon_1'' = -\varepsilon_2''$. The real parts are generally $\varepsilon_1' = \pm\varepsilon_2'$. Moreover, we get a condition on the thickness of slabs as $\rho_1 = \rho_2$. Thus balancing loss and gain for the planar bilayer requires permittivities $\varepsilon_1 = \varepsilon_1' + i\varepsilon_1''$ and $\varepsilon_2 = \pm\varepsilon_1' - i\varepsilon_1''$ of the layers of the same thickness $d_1 = d_2$. In the case $\varepsilon_1' = \varepsilon_2'$, we approach a famous result used in a plenty of works on $\mathcal{PT}$-symmetric multilayers, e.g., in Refs. [47,48]. In Ref. [49], we went beyond the local EMA to adequately describe exceptional points in such systems. Notice that for the layers $a \leqslant z \leqslant c$ and $c < z \leqslant b$, the condition $\rho_1 = \rho_2$ allows us to determine the position c of the interface as $c = (a + b)/2$.

The case $\varepsilon_1' = -\varepsilon_2'$ can be realized for two layers, one of which is attenuating metal ($\varepsilon_1 = -|\varepsilon_1'| + i|\varepsilon_1''|$), while the other slab is amplifying dielectric ($\varepsilon_1 = |\varepsilon_1'| - i|\varepsilon_1''|$).

Spherical bilayer. From Eq. (43), we readily derive

$$\frac{\rho_2'}{\rho_2}|\varepsilon_1|^2 = \frac{\rho_1'}{\rho_1}|\varepsilon_2|^2\tag{44}$$

or

$$\frac{\rho_2'}{\rho_2}\left(\varepsilon_1'^2+\varepsilon_1''^2\right) = \frac{\rho_1'}{\rho_1}\left(\varepsilon_2'^2+\frac{\rho_1^2}{\rho_2^2}\varepsilon_1''^2\right).\tag{45}$$

In order to disentangle the real and imaginary parts of permittivities, we demand

$$\rho_1\rho_1' = \rho_2\rho_2'.\tag{46}$$

This equation can be solved with respect to the radius c of the interface between two spherical layers. Indeed, we get

$$(c-a)(a^{-1}-c^{-1}) = (b-c)(c^{-1}-b^{-1})\tag{47}$$

that results in

$$c = \sqrt{ab}.\tag{48}$$

So, the value c should be the geometric mean of the inner and outer radii, in contrast to the arithmetic mean for planar layers. The ratio of filling fractions then equals $\rho_1/\rho_2 = \sqrt{a/b}$. From Eq. (45), we also find the connection between the real parts of permittivity,

$$\varepsilon_2' = \pm\varepsilon_1' \frac{\rho_1}{\rho_2} = \pm\varepsilon_1' \sqrt{\frac{a}{b}}. \tag{49}$$

Taking the sign "+," we obtain the permittivities of unequal spherical layers needed to balance loss and gain as $\varepsilon_1 = \varepsilon_1' + i\varepsilon_1''$ for $a \leqslant r \leqslant c$ and $\varepsilon_2 = (\rho_1/\rho_2)(\varepsilon_1' - i\varepsilon_1'') = \sqrt{a/b}(\varepsilon_1' - i\varepsilon_1'')$ for $c < r \leqslant b$.

The material parameters and position of the interface for spherical layers reduce to those for planar layers in the limit of thin layers compared to their radii, $(b - c), (c - a) \ll c$. For waves propagating in the cylinder cross-section, the material parameters of balanced layers can be calculated similarly to those of spherical layers.

VII. CONCLUSION

We propose the operator effective medium approximation for spherically and cylindrically symmetric multilayer systems. In contrast to the operator EMA developed earlier for planar multilayers, here we use the Born series expansion for the evolution operator giving the fundamental solution of the Maxwell equations in spherical or cylindrical coordinates. Effective material parameters are derived from the equality of the evolution operators of the multilayer system and effective medium. Doing so, we have derived the local effective dielectric permittivity tensor of a nonmagnetic nonchiral multilayer. To verify the operator EMA, we have calculated the scattering efficiencies for dielectric and metallic structures. For the cylindrical system, we have determined two sets of effective material parameters, the first of which includes only the local permittivity tensor, while the second set provides permittivity and wavenumber-dependent permeability tensors. Comparison of these two sets of effective material parameters unveils the benefits of exploitation of local material parameters. We have clarified the criterion of EMA validity supplementing the requirement of subwavelength layers with the condition on the curvature of the layers that should be about or smaller than the inverse wavelength. Finally, requiring reality of the effective material parameters, we have found the parameters of spherical bilayer with balanced loss and gain.

ACKNOWLEDGMENTS

Study on balanced loss and gain layers was supported by the Russian Science Foundation (Project No. 21-12-00383). M.R. and D.V.N. are grateful to the State Program of Scientific Research "Photonics and Electronics for Innovations" (Task 1.5).

[1] Y. Liu and X. Zhang, Metamaterials: A new frontier of science and technology, Chem. Soc. Rev. **40**, 2494 (2011).
[2] N. I. Zheludev and Y. S. Kivshar, From metamaterials to metadevices, Nat. Mater. **11**, 917 (2012).
[3] M. Kadic, G. W. Milton, M. van Hecke, and M. Wegener, 3D metamaterials, Nat. Rev. Phys. **1**, 198 (2019).
[4] T. C. Choy, *Effective Medium Theory: Principles and Applications* (Oxford Academic, Oxford, 2016).
[5] C. R. Simovski, On electromagnetic characterization and homogenization of nanostructured metamaterials, J. Opt. **13**, 013001 (2011).
[6] R. Ruppin, Evaluation of extended Maxwell-Garnett theories, Opt. Commun. **182**, 273 (2000).
[7] V. A. Markel, Introduction to the Maxwell Garnett approximation: tutorial, J. Opt. Soc. Am. A **33**, 1244 (2016).
[8] V. A. Markel, Maxwell Garnett approximation (advanced topics): tutorial, J. Opt. Soc. Am. A **33**, 2237 (2016).
[9] V. A. Markel, Maxwell Garnett approximation in random media: tutorial, J. Opt. Soc. Am. A **39**, 535 (2022).
[10] Y. Liu, S. Guenneau, and B. Gralak, Artificial dispersion via high-order homogenization: magnetoelectric coupling and magnetism from dielectric layers, Proc. R. Soc. A. **469**, 20130240 (2013).
[11] H. H. Sheinfux, I. Kaminer, Y. Plotnik, G. Bartal, and M. Segev, Subwavelength multilayer dielectrics: Ultrasensitive transmission and breakdown of effective-medium theory, Phys. Rev. Lett. **113**, 243901 (2014).
[12] A. Andryieuski, A. V. Lavrinenko, and S. V. Zhukovsky, Anomalous effective medium approximation breakdown in deeply subwavelength alldielectric photonic multilayers, Nanotechnology **26**, 184001 (2015).
[13] S. V. Zhukovsky, A. Andryieuski, O. Takayama, E. Shkondin, R. Malureanu, F. Jensen, and A. V. Lavrinenko, Experimental demonstration of effective medium approximation breakdown in deeply subwavelength all-dielectric multilayers, Phys. Rev. Lett. **115**, 177402 (2015).
[14] X. Lei, L. Mao, Y. Lu, and P. Wang, Revisiting the effective medium approximation in all-dielectric subwavelength multilayers: Breakdown and rebuilding, Phys. Rev. B **96**, 035439 (2017).
[15] S. Yuan, X. Zhou, Y. Chen, Y. Zhong, L. Sheng, H. Hu, H. Chen, I. Kaminer, and X. Lin, Breakdown of effective-medium theory beyond the critical angle, Sci. China Phys. Mech. & Astro. **66**, 114212 (2023).
[16] V. Popov, A. V. Lavrinenko, and A. Novitsky, Operator approach to effective medium theory to overcome a breakdown of Maxwell Garnett approximation, Phys. Rev. B **94**, 085428 (2016).
[17] U. K. Chettiar and N. Engheta, Internal homogenization: Effective permittivity of a coated sphere, Opt. Express **20**, 22976 (2012).
[18] B. A. Slovick, Z. G. Yu, and S. Krishnamurthy, Generalized effective-medium theory for metamaterials, Phys. Rev. B **89**, 155118 (2014).
[19] T. Geng, S. Zhuang, J. Gao, and X. Yang, Nonlocal effective medium approximation for metallic nanorod metamaterials, Phys. Rev. B **91**, 245128 (2015).
[20] B. A. Slovick, Negative refractive index induced by percolation in disordered metamaterials, Phys. Rev. B **95**, 094202 (2017).
[21] A. A. Siraji and Y. Zhao, Simple effective medium approximation with Rayleigh scattering, Opt. Lett. **42**, 1860 (2017).
[22] K. Mnasri, F. Z. Goffi, M. Plum, and C. Rockstuhl, Homogenization of wire media with a general purpose nonlocal constitutive relation, J. Opt. Soc. Am. B **36**, F99 (2019).
[23] C. P. Mavidis, A. C. Tasolamprou, E. N. Economou, C. M. Soukoulis, and M. Kafesaki, Single scattering and effective

medium description of multilayer cylinder metamaterials: Application to graphene- and to metasurface-coated cylinders, Phys. Rev. B **107**, 134120 (2023).
[24] A. Alú, First-principles homogenization theory for periodic metamaterials, Phys. Rev. B **84**, 075153 (2011).
[25] A. Ciattoni, D. Rago, and C. Rizza, Separable metamaterials: analytical *ab-initio* homogenization and chirality, J. Opt. **18**, 115103 (2016).
[26] S. Lannebere, T. A. Morgado, and M. G. Silveirinha, First principles homogenization of periodic metamaterials and application to wire media, Comptes Rendus. Physique **21**, 367 (2020).
[27] R. Venkitakrishnan, T. Höß, T. Repän, F. Z. Goffi, M. Plum, and C. Rockstuhl, Lower limits for the homogenization of periodic metamaterials made from electric dipolar scatterers, Phys. Rev. B **103**, 195425 (2021).
[28] I. Tsukerman, Nonlocal homogenization of metamaterials by dual interpolation of fields, J. Opt. Soc. Am. B **28**, 2956 (2011).
[29] A. Ciattoni and C. Rizza, Nonlocal homogenization theory in metamaterials: Effective electromagnetic spatial dispersion and artificial chirality, Phys. Rev. B **91**, 184207 (2015).
[30] M. A. Gorlach, T. A. Voytova, M. Lapine, Y. S. Kivshar, and P. A. Belov, Nonlocal homogenization for nonlinear metamaterials, Phys. Rev. B **93**, 165125 (2016).
[31] K. Mnasri, A. Khrabustovskyi, C. Stohrer, M. Plum, and C. Rockstuhl, Beyond local effective material properties for metamaterials, Phys. Rev. B **97**, 075439 (2018).
[32] Y. Zhong, T. Cai, T. Low, H. Chen, and X. Lin, Optical interface engineering with on-demand magnetic surface conductivities, Phys. Rev. B **106**, 035304 (2022).
[33] X. Zhang, J. Chen, R. Chen, C. Wang, T. Cai, R. Abdi-Ghaleh, H. Chen, and X. Lin, Perspective on meta-boundaries, ACS Photonics **10**, 2102 (2023).
[34] X.-X. Liu and A. Alú, Generalized retrieval method for metamaterial constitutive parameters based on a physically driven homogenization approach, Phys. Rev. B **87**, 235136 (2013).
[35] S. Arslanagic, T. V. Hansen, N. A. Mortensen, A. H. Gregersen, O. Sigmund, R. W. Ziolkowski, and O. Breinbjerg, A review of the scattering-parameter extraction method with clarification of ambiguity issues in relation to metamaterial homogenization, IEEE Ant. Prop. Mag. **55**, 91 (2013).
[36] V. Grigoriev, G. Demesy, J. Wenger, and N. Bonod, Singular analysis to homogenize planar metamaterials as nonlocal effective media, Phys. Rev. B **89**, 245102 (2014).
[37] A. Castanie, J.-F. Mercier, S. Felix, and A. Maurel, Generalized method for retrieving effective parameters of anisotropic metamaterials, Opt. Express **22**, 29937 (2014).
[38] A. F. Mota, A. Martins, J. Weiner, F. L. Teixeira, and B.-H. V. Borges, Constitutive parameter retrieval for uniaxial metamaterials with spatial dispersion, Phys. Rev. B **94**, 115410 (2016).
[39] S. Larouche and V. Radisic, Retrieval of all effective susceptibilities in nonlinear metamaterials, Phys. Rev. A **97**, 043863 (2018).
[40] V. Popov, A. V. Lavrinenko, and A. Novitsky, Surface waves on multilayer hyperbolic metamaterials: Operator approach to effective medium approximation, Phys. Rev. B **97**, 125428 (2018).
[41] L. M. Barkovskii, G. N. Borzdov, and A. V. Lavrinenko, Fresnel's reflection and transmission operators for stratified gyroanisotropic media, J. Phys. A: Math. Gen. **20**, 1095 (1987).
[42] G. N. Borzdov, Frequency domain wave-splitting techniques for plane stratified bianisotropic media, J. Math. Phys. **38**, 6328 (1997).
[43] A. Novitsky and L. Barkovsky, Matrix approach for light scattering from a multilayered rotationally symmetric bianisotropic sphere, Phys. Rev. A **77**, 033849 (2008).
[44] F. I. Fedorov, *Theory of Gyrotropy* (Nauka i Tehnika, Minsk, 1976).
[45] A. V. Novitsky and L. M. Barkovsky, Operator matrices for describing guiding propagation in circular bianisotropic fibres, J. Phys. A: Math. Gen. **38**, 391 (2005).
[46] A. V. Novitsky, Matrix approach for light scattering by bianisotropic cylindrical particles, J. Phys.: Condens. Matter **19**, 086213 (2007).
[47] Y. D. Chong, Li Ge, and A. D. Stone, $\mathcal{PT}$-symmetry breaking and laser-absorber modes in optical scattering systems, Phys. Rev. Lett. **106**, 093902 (2011).
[48] L. Ge, Y. D. Chong, and A. D. Stone, Conservation relations and anisotropic transmission resonances in one-dimensional $\mathcal{PT}$-symmetric photonic heterostructures, Phys. Rev. A **85**, 023802 (2012).
[49] D. V. Novitsky, A. S. Shalin, and A. V. Novitsky, Nonlocal homogenization of PT-symmetric multilayered structures, Phys. Rev. A **99**, 043812 (2019).